Fines Removal in a Continuous Plug Flow Crystallizer by Optimal Spatial Temperature Profiles with Controlled Dissolution

Aniruddha Majumder
Dept. of Chemical Engineering, Loughborough University, Loughborough LE11 3TU, U.K.

Zoltan K. Nagy
School of Chemical Engineering, Purdue University, West Lafayette, IN 47907

Dept. of Chemical Engineering, Loughborough University, Loughborough LE11 3TU, U.K.

DOI 10.1002/aic.14196
Published online August 1, 2013 in Wiley Online Library (wileyonlinelibrary.com)

This work presents a systematic study for obtaining the optimal temperature profile in a continuous plug flow crystallizer (PFC). The proposed PFC consists of multiple segments where the temperature of each segment can be controlled individually. An optimization problem is formulated for a target crystal size distribution (without fines) with the temperature of the segments as decision variables. The results indicate that for the crystallization kinetics considered, dissolution steps are necessary for the reduction of fines due to nucleation. A systematic study on the form of growth and dissolution kinetics suggested that the key factor that determines whether the dissolution steps will be successful in reducing fines, without compromising the final size of the crystals from seed, is the size dependence of the growth and dissolution kinetics. Best fines removal is achieved when the larger crystals grow faster than the smaller ones and the smaller crystals dissolve faster than the larger ones. © 2013 American Institute of Chemical Engineers *AIChE J*, 59: 4582–4594, 2013

Keywords: control of continuous crystallizer, fines removal, optimal temperature profile, plug flow crystallizer, population balance modeling

Introduction

Crystallization is a key unit operation widely used as a means of separation and purification in chemical, food, and pharmaceutical industries. More than 90% of the active pharmaceutical ingredients in pharmaceutical industry are crystals of some organic materials.[1] Traditionally crystallization has been operated as batch processes which have several drawbacks such as reduced flexibility in control, large processing time, and scale-up issues. Conversely, continuous processing has been envisaged as a key element in improving manufacturing in pharmaceutical industries due to several benefits such as: consistency of product quality, shorter down time, and reduced manufacturing cost by improving asset utilization.[2] As an example, significant improvement in terms of processing time and expenses have been reported in the literature for a model compound in the continuous oscillatory baffled crystallizer as compared to a batch process.[3] However, one needs to balance these advantages against specific drawbacks that the continuous processing may have, such as the slow attainment of steady state, incrustation problems, and potential instability of operation.[4]

Correspondence concerning this article should be addressed to Z. K. Nagy at zknagy@purdue.edu.

Crystal size distribution (CSD) plays a key role in determining the dissolution profile and consequently bioavailability of the administered drug. Thus, stringent control over CSD is required for the desired bioavailability and the method of drug administration.[5] Control over CSD is also necessary for efficient operation of the downstream processes such as filtration and drying. It is a well known fact that in a batch crystallization process, optimal, or programmed cooling profiles can provide better control over the CSD than linear or natural cooling by reducing fines due to nucleation.[6–8] Typically in such profiles the temperature of the system is decreased slowly at the beginning and at a faster rate toward the end of the batch to promote growth. Although by maintaining such temperature profile one can increase the mean size of the crystals and reduce the fines to some extent, complete removal of the fines may not be possible.[7–9] One way to eliminate the fines is to recycle the classified stream of slurry containing fines, obtained from a elutriation leg or settling zone of the draft tube crystallizer, through a heating pipe to dissolve the fines.[10,11] In recent years, the *in situ* fines removal technique by temperature cycling that does not require any extra dissolution unit has been shown to work successfully in removing fines for batch processes.[8,12–15] This *in situ* fines removal technique can be implemented either using a model free (direct design) approach[8,13–16] or a model-based approach.[8,17,18] In a model free approach, the

real time measurements provided by process analytical technology is used to adapt the operating policies to control growth, dissolution, and nucleation events. Conversely, in model-based approaches the optimal temperature profile is followed that is obtained by solving the model equations describing the crystallization process.[19–24] It has been further shown that under certain conditions, dissolution step may be essential to match the unimodal target CSD without fines by considering the batch cooling crystallization of potash alum in water.[8]

In this work, we extend the model-based *in situ* fines removal technique by Nagy et al.[8] to continuous crystallization process. Cooling crystallization of a model compound in a continuous plug flow crystallizer (PFC) is considered. A framework suitable for the simultaneous design and optimal control of PFC system is proposed. According to this framework, the PFC consists of M modules or segments where the temperature of each segment can be controlled separately. In this approach, the structure of the alternating cooling and heating elements and overall temperature profile is determined for optimal control performance. The optimal temperature profile is obtained by formulating and solving an optimization problem. It is found that dissolution steps are necessary for achieving a target CSD without fines for the kinetics considered. The steady state crystallization process is modeled using population balance equations (PBEs).[25] Due to the complexity and nonlinearity of the PBEs describing crystallization processes, the gradient-based optimization technique are often not suitable for solving such optimization problem as they may fail to find the global optimum. Conversely stochastic techniques, despite of being computationally more expensive than the gradient-based techniques, are better suited (although not guaranteed) for finding the global optimum. Some hybrid techniques have also been developed which combine the efficiency of gradient-based local nonlinear programming (NLP) solvers with the stochastic technique for global search.[26] In this work, we use the genetic algorithm (GA) that is available at the global optimization toolbox in Matlab. Although global optimality is not guaranteed in GA, it is found to provide better results than the hybrid techniques for the case studies considered. We further perform a systematic study on the ability of the growth and dissolution kinetics in removing fines. This study suggests that size dependence of the growth and dissolution kinetics play an important role in determining how successful the optimal profile would be to remove the fines. It is found that the best results in terms of fines removal can be obtained when both the growth and dissolution rates are functions of crystal size, that is, when larger particles grow faster than the smaller ones and the smaller particles dissolve faster than the larger ones. However, when both the growth and dissolution rates are size independent, the dissolution steps are found to be ineffective in removing fines.

Population balance modeling is used to model the crystallization process.[25] Due to the complexity of the PBEs, numerical solution is required in most practical cases. There is a range of techniques that are used to solve the PBEs. Some of them aim to provide efficient solution in terms of moments of the distribution for application in online model-based control, such as method of moments[27] and quadrature method of moments.[28–30] Conversely, various techniques are available that provide solutions of the PBE in terms of the CSD, such as high resolution finite volume (FV) method,[11,31–33] weighted essentially nonoscillatory method,[34,35] finite element method,[36,37] method of characteristics,[38,39] and lattice Boltzmann method.[40–42] In this article, we use high resolution FV method for solving the resulting PBEs for its accuracy, ease of implementation, and robustness.

The article is organized as follows: In the second section, the steady state modeling of the PFC is discussed using coupled PBEs that account for crystal growth, nucleation, and dissolution. In the third section, details of the high resolution FV technique are presented. In the fourth section, formulation of the optimization problem is discussed. In the fifth section, simulation results and discussions are presented for various types of growth and dissolution kinetics. In the sixth section, a case study is considered that affirms the effectiveness of the proposed multisegment crystallizer design and temperature profile in reducing fines. Finally, some concluding remarks are made in the seventh section.

Modeling of PFC

The PFC is one of the most commonly used continuous crystallizers. In a PFC, solution is fed at the inlet and supersaturation is generated by cooling or antisolvent addition as the solution moves through the tube. Due to the generation of supersaturation, crystallization takes place, and the product crystals are collected at the outlet. Various types of static and moving baffled systems are available to ensure mixing of the solution inside a PFC and to achieve plug flow conditions as closely as possible.[1,3]

The schematic of the PFC used in this study is shown in Figure 1. It is assumed that there is perfect mixing of the slurry in the radial direction, and there is no mixing or dispersion in the axial direction. The PFC consists of M number of modules or segments. Based on the process requirements, the number of the segments can be increased or decreased by fitting or removing segments. Temperature of each segment can be controlled independently. The steady state PBEs that describe the crystallization process in the PFC has the following form[1]

$$\text{PBE} \quad \text{when} \quad S \geq 0 : u_x \frac{\partial f_n}{\partial x} + \frac{\partial}{\partial L}(G f_n) = 0; \tag{1}$$

$$\text{B.C.} : G(S,L) f_n(L,x)|_{L=0} = B_0(S), \tag{2}$$

$$f_n(L,x)|_{x=0} = f_{n,\text{seed}}(L); \tag{3}$$

$$\text{PBE} \quad \text{when} \quad S < 0 : u_x \frac{\partial f_n}{\partial x} - \frac{\partial}{\partial L}(D f_n) = 0; \tag{4}$$

$$\text{B.C.} : D(S,L) f_n(L,x)|_{L=L_{\max}} = 0, \tag{5}$$

$$f_n(L,x)|_{x=0} = f_{n,\text{seed}}(L); \tag{6}$$

$$\text{Kinetics} : G(S,L) = k_g S^g (1+\gamma L)^p; \tag{7}$$

$$D(S,L) = \frac{k_d}{L^q}(-S)^d; \tag{8}$$

$$B_0(S) = k_b S^b \mu_3; \tag{9}$$

$$S = (C - C_{\text{sat}}); \tag{10}$$

where $f_n(L,x)$ is the number-based CSD, $f_{n,\text{seed}}(L)$ is the seed distribution, u_x is the mean flow velocity calculated as $u_x = Q/A$ where Q is the volumetric flow rate and A is the cross sectional area of the crystallizer, $G(S,L)$ is the growth rate, $D(S,L)$ is the dissolution rate, x is the spatial position along the crystallizer, L is the crystal size, S is the absolute supersaturation, C is the concentration, B_0 is the nucleation

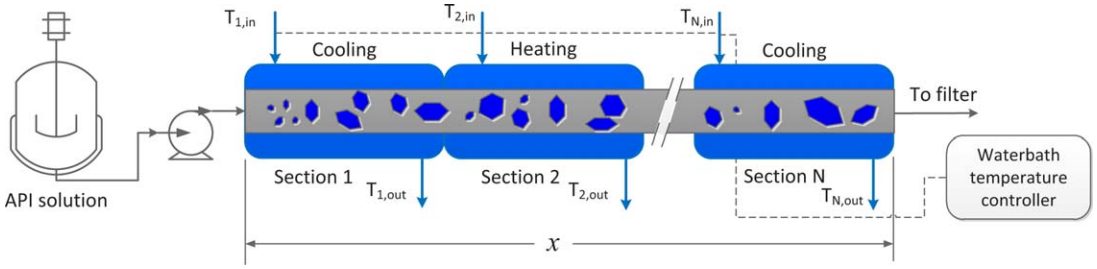

Figure 1. Schematic diagram of PFC showing heating and cooling sections.

[Color figure can be viewed in the online issue, which is available at wileyonlinelibrary.com.]

rate, μ_3 is the third moment of CSD, and k_g, g, p, k_d, d, q, γ, k_b, b are kinetic parameters. Crystal growth, dissolution, and nucleation kinetics in a crystallizer are expressed as functions of supersaturation, either absolute or relative, by empirical formula. In this work, we use absolute supersaturation as the parameters for growth are taken for potash alum-water system reported by Aamir et al.[7] where the kinetic expression is expressed in terms of absolute supersaturation. The growth rate expression of the crystals used in Eq. 7 is size dependent to highlight the fact that some crystals are reported to exhibit size dependent growth rate.[8,31,43,44] For size independent growth rate the parameter $\gamma = 0$ can be used. Although intrinsically the crystal growth may be independent of crystal size, the apparent manifestation of size dependent growth rate of some crystals is explained by McCabe and Stevens[45] and Abegg et al.[43] In most crystallization processes, where heat of crystallization is relatively low, there are two major steps involved in the growth process: transport of the solute molecules from the bulk to the crystal face and subsequent integration of the solute molecules on the crystal face by surface reaction. The diffusion resistance is low in most crystallization systems and the growth is controlled by surface reaction.[43] In such cases, the growth rate is found to be size independent. However, if the growth rate is diffusion controlled, size dependent growth rate may be manifested. This is due to the fact that larger crystals have higher settling velocity (i.e., greater relative crystal-solution velocity) which results in decrease in diffusion boundary layer and diffusion resistance. Similar conclusions are made in a more recent study by Kile and Eberl.[44] More often the cause of apparent size dependent growth can be growth rate dispersion.[46,47] However, in this case a size dependent growth rate expression is often applied as an empirical equation to describe the evolution of the experimental CSD.

Conversely, the fine crystals are reported to have higher solubility than the larger ones and will dissolve preferentially.[48] However, this increase in solubility of the fine crystals is often appreciable when the size is less than few micrometers.[49] Similar to the growth process, the dissolution of the crystals involves two major steps, that is, detachment of the solute molecules from the crystal surface, followed by transport of the solute molecules by diffusion. Between the two steps, mass transfer is usually assumed to determine the dissolution rate as the detachment of the solute from crystal surface is faster.[49] The dissolution kinetics in Eq. 8 is also taken to be size dependent. This size dependence is believed to be resulting mainly from the size dependence of the mass transfer coefficient.[50,51]

In addition to the PBEs and kinetic equations given by Eqs. 1–9, one needs to take into account the rate of depletion or increment of the solute in the solution at any location along the PFC. This depletion of solute is equal to the mass gained by the crystals due to growth assuming that the size of the nuclei is negligible. Conversely, increment of solute in the solution at any location can be obtained by considering the rate of mass lost by the crystals due to dissolution. Thus, the mass balance equation can be written as[1]

$$u_x \frac{dC}{dx} = -3\rho_c k_v G \int L^2 f_n dL, \text{ when } \quad S \geq 0; \tag{11}$$

$$u_x \frac{dC}{dx} = 3\rho_c k_v D \int L^2 f_n dL, \text{ when } \quad S < 0; \tag{12}$$

where ρ_c is the density of the crystals and k_v is the volume shape factor. When heat of crystallization is negligible, the PBEs and kinetic equations coupled with mass balance complete the description of crystallization process. In most practical cases, the model equations have to be solved numerically. The high resolution FV technique that has been used in this article is discussed briefly in the next section.

High Resolution FV Method for Solving PBEs

The high resolution FV technique used in this work is the combination of the semidiscrete FV technique with the van Leer flux limiter.[52] FV methods are a class of discretized methods for solving partial differential equations (PDEs) representing conservation laws. As opposed to finite difference methods, which approximate the underlying PDE by forward or backward differences, FV methods are based on the integral form of the conservation law. The computational domain is discretized into N grid cells and the average value of the conserved variable is tracked in each cell. The advantage of this integral form of the conservation law is that it holds even for discontinuous solutions, whereas the differential form does not.[53] The discretization of the computational domain in FV method is shown in Figure 2.

The average quantity in each cell is defined as

$$f_{n,i} = \frac{1}{\Delta L} \int_{L_{i-1/2}}^{L_{i+1/2}} f_n dL, \tag{13}$$

where ΔL is the cell width. With this definition, by integrating the PBE given by Eq. 1 in the ith cell we obtain the following set of ordinary differential equations (ODEs).

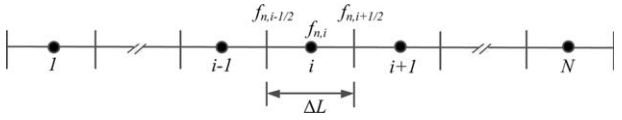

Figure 2. Schematic representation of the FV discretization.

$$\frac{df_{n,i}}{dx} = -\frac{1}{u_x \Delta L}\left(G_{i+1/2} f_{n,i+1/2} - G_{i-1/2} f_{n,i-1/2}\right), \quad (14)$$

where the flux $G_{i+1/2} f_{n,i+1/2}$ at the cell boundary needs to be evaluated from the available cell average values. The accuracy of the FV method depends on the way in which the cell-face fluxes are computed. Generally, a Taylor series expansion or piecewise polynomial interpolation is used to determine the fluxes at the cell-face. Moreover, flux limiter functions are often used to avoid the spurious oscillations (wiggles) that would otherwise occur with high-order spatial discretization schemes due to shocks, discontinuities, or sharp changes in the solution domain. The role of flux limiter function is essentially to switch between higher order and lower order flux approximation of the cell-face flux for smooth and nonsmooth solutions, respectively. The expression for $f_{n,i+1/2}$ required for flux approximation is written as

$$f_{n,i+1/2} = f_{n,i} + \frac{1}{2}\phi\left(r_{i+1/2}\right)\left(f_{n,i+1} - f_{n,i}\right), \quad (15)$$

where the flux limiter function $\phi\left(r_{i+1/2}\right)$ depends on the smoothness of the distribution, which is quantified by the ratio of the gradients of the solution in two consecutive cells as follows[31]

$$r_{i+1/2} = \frac{f_{n,i} - f_{n,i-1} + \epsilon}{f_{n,i+1} - f_{n,i} + \epsilon}, \quad (16)$$

where $\epsilon = 10^{-10}$ is a small number to avoid division by zero. Some widely used flux limiters are van Leer,[52] Koren,[54] Superbee,[55] and minimod.[55] When such flux limiter functions are used, the scheme is known as high resolution method. In this study, we use van Leer flux limiter which is reported to work well for PBEs.[31]

$$\phi\left(r_{i+1/2}\right) = \frac{r_{i+1/2} + |r_{i+1/2}|}{1 + |r_{i+1/2}|} \quad (17)$$

Note that the flux approximation given by Eq. 15 is not applicable at the boundary cells. For example, evaluation of $f_{n,1+1/2}$ would require $f_{n,0}$ which is non existent. This problem is typically overcome by first-order approximation for $f_{n,1+1/2}$ and $f_{n,N+1/2}$ as follows

$$f_{n,1+1/2} = \frac{f_{n,1} + f_{n,2}}{2}; \; f_{n,N+1/2} = f_{n,N}. \quad (18)$$

The flux at the inlet boundary is obtained from boundary condition

$$G_{1/2} f_{n,1/2} = B_0. \quad (19)$$

Although in the above discussion the high resolution FV method is presented for solving Eq. 1, that is, PBEs with growth and nucleation, the technique can be easily adapted for solving PBEs with dissolution which can be summarized as

$$\text{if } i = 0 : f_{n,1/2} = f_{n,1}, \quad (20)$$

$$\text{if } 1 \le i \le N-2 : f_{n,i+1/2} = f_{n,i+1} + \frac{1}{2}\phi\left(r_{i+1/2}\right)\left(f_{n,i} - f_{n,i+1}\right), \quad (21)$$

$$\text{if } i = N-1 : f_{n,N-1/2} = \frac{f_{n,N} + f_{n,N-1}}{2}, \quad (22)$$

$$\text{if } i = N : f_{n,N+1/2} = 0, \quad (23)$$

$$r_{i+1/2} = \frac{f_{n,i+1} - f_{n,i+2} + \epsilon}{f_{n,i} - f_{n,i+1} + \epsilon}. \quad (24)$$

Finally, the resulting set of ODEs can be solved by any accurate and efficient solver. In this work, an explicit fourth-order Runge-Kutta ODE solver is used for solving the resulting set of ODEs. The technique is implemented in the "ode45" solver available in Matlab.

Formulation of the Optimization Problem for the Multisegment Continuous PFC

In this section, we formulate the optimization problem which is solved for obtaining optimal temperature profiles for the multisegment PFC considering nucleation, growth, and dissolution. First, a target unimodal distribution without fines is defined. Typically volume-based CSD $\left(f_{v,i}\right)$ is used for this purpose as it can be obtained from experiments

$$f_{v,i} = \frac{f_{n,i} L_i^3}{\sum_{i=1}^{N} f_{n,i} L_i^3 \Delta L_i}. \quad (25)$$

Then, an objective function (J) to be minimized is defined by taking sum of the squared difference of the target CSD and CSD obtained from the final section of the crystallizer. The decision variables (T_j) are the inlet temperature of each segment. The outlet temperature of the preceding segment is taken the same as the inlet temperature of the succeeding segment. The upper and lower bounds of the decision variables are fixed as $T_{max} = 40°C$ and $T_{min} = 10°C$, respectively and the temperature of the feed solution is fixed at 40°C. In order to make sure that the temperature profile is practically implementable, a constraint is imposed on the decision variables that the difference of the inlet and outlet temperatures can be 5°C at maximum. The temperature profile along the PFC is approximated by assuming that in each segment the temperature follows an exponential profile starting from inlet temperature to reach the outlet temperature as follows

$$T = T_j - \left(T_j - T_{j+1}\right)\left[1 - \exp\left(-\frac{x/x_s - (j-1)}{0.15}\right)\right], \quad (26)$$

where T_j is the inlet temperature in °C of the jth segment, x_s is length of a PFC segment, and the parameter in the exponent is chosen arbitrarily. This approximation simulates the real temperature profile within a single segment with constant input temperature. The optimization problem is

$$\min_{T_j} \; J = \sum_{i=1}^{N} \lambda_i \left(f_{v,i}^t - f_{v,i}\right)^2, \quad (27)$$

$$\text{subject to : Model equations 1–9} \quad (28)$$

$$T_{min} \le T_j \le T_{max}, \quad (29)$$

$$-5\,°C \le T_{j+1} - T_j \le 5\,°C \quad (30)$$

here λ_i is a scaling factor, $f_{v,i}^t$ is the volume-based target CSD in the size range belonging to the ith cell.

The optimization problem Eqs. 27–30 is strongly nonlinear with relatively large number of decision variables. Additionally, the solution of the coupled PBEs describing the process may lead to discontinuity in the solution. This kind of problems are often too complex to be solved using deterministic techniques such as gradient (Jacobian)-based methods. Evolutionary algorithms such as GA has shown increased usefulness for such optimization problems. The advantages of GA over the gradient-based techniques are that GA requires little

Table 1. Kinetic Parameters for the Model Compounds

Parameter	Value	Units
k_b	0.0380×10^2	#/(μm/s)
B	3.4174	Dimensionless
k_g	8.5708	μm/s
g	1	Dimensionless
γ	0.005	/μm
p	1.5778	Dimensionless
k_d	10.7192	μm/s
d	0.5122	Dimensionless
q	0.3382	Dimensionless
ρ_c	1.75×10^{-12}	g/μm^3

The growth and nucleation kinetics are taken from Aamir et al.[7] where k_b is taken as 100 times. The dissolution kinetics is fictitious.

knowledge about the problem being solved, it is easy to implement, robust, and inherently parallel.[56] To be able to evaluate the objective (cost) function for a given set of input parameters is sometimes what is only required. In this article, we use the GA tool available in the Matlab global optimization toolbox for solving the optimization problem. We have also compared the results obtained using GA with that obtained using hybrid techniques with multiple starting points. GA is found to be working well in our case. A comparison of the study can be found in the subsequent section.

Study of the Optimal Temperature Profiles for Various Types of Growth and Dissolution Kinetics

In this section, we consider cooling crystallization of a model compound in a PFC. The aim is to determine the optimal temperature trajectory which yields crystals with target unimodal CSD from the final segment of the PFC. The dimension of each segment is taken as length 200 mm, internal diameter 12.7 mm. The volumetric flow rate of the slurry is $8.33\times10^2\text{mm}^3/\text{s}$. The kinetic parameters used in the simulation are given in Table 1.

The seed distribution is taken as a Gaussian with mean of 54 μm and standard deviation of 15 μm

$$f_{n,\text{seed}}\left[\#/\mu\text{m}^2\right]=\frac{5\times10^4}{15\sqrt{2\pi}}\exp\left(-\frac{(L-54)^2}{15^2}\right). \quad (31)$$

The unimodal target CSD is obtained by following a linear cooling profile from 40 to 10°C and arbitrarily setting nucleation to zero. The scaling factor is taken as $\lambda_i=10^5$ μm^2. The solubility of the compound is taken to be same as potash alum in water[8]

$$C_{\text{sat}}\left[\text{g/g of solvent}\right]=3.583545\times10^{-5}T^2+2.431836\times10^{-4}T+3.633927\times10^{-2}. \quad (32)$$

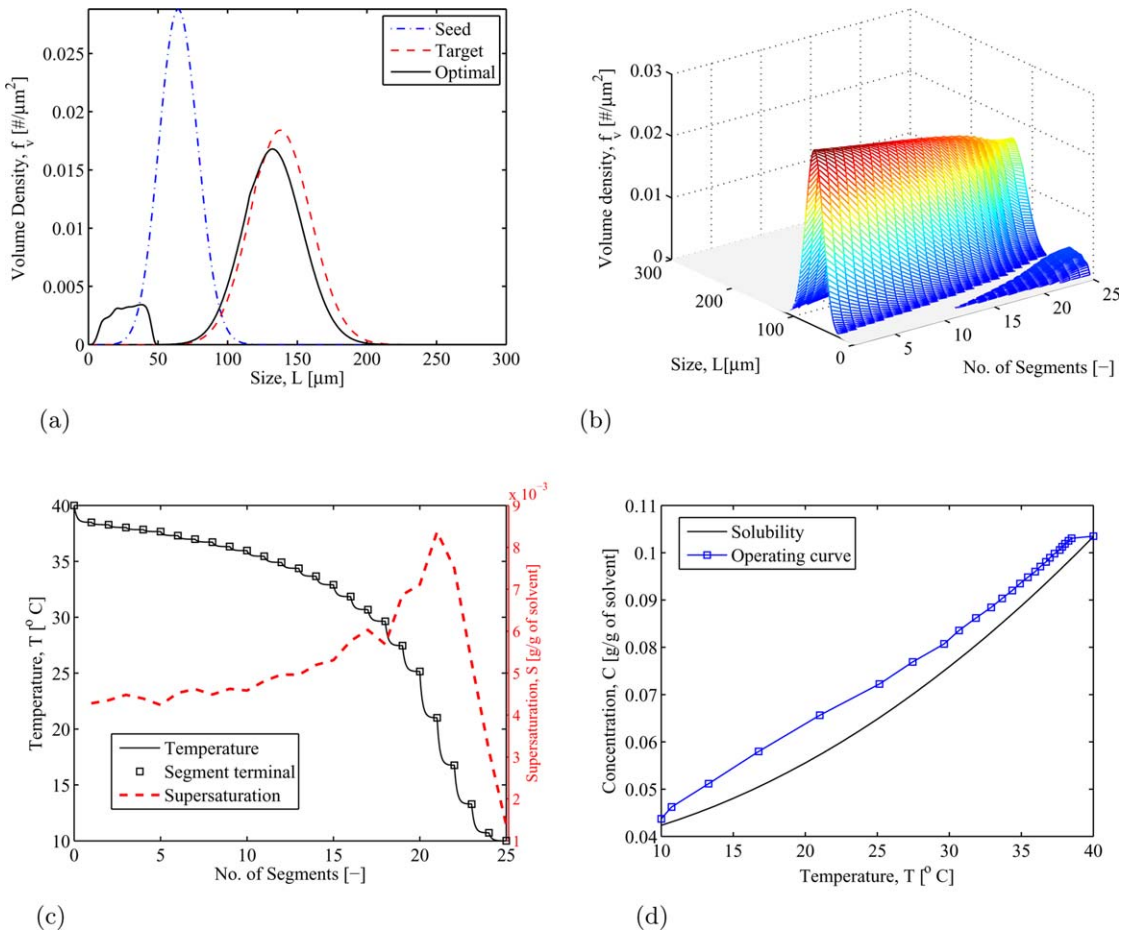

Figure 3. Optimization results when no dissolution steps are present.

(a) Final distribution. (b) Evolution of the CSD along the crystallizer segments. (c) Temperature and supersaturation profile. (d) Operating curve in the phase diagram. [Color figure can be viewed in the online issue, which is available at wileyonlinelibrary.com.]

Table 2. Summary of the Optimization Results

Dissolution	Case	Pop. Size [-]	No. of Gen. [-]	CPU Time [min]	J [-]
Not considered	1	100	87	43.78	85.39
Considered	1	50	198	100	17.57
	2	50	196	35	446.97
	3	100	128	77	327.30

The initial concentration is taken as the saturation concentration at 40°C. Number of grid points used for size discretization is $N = 300$. The GA parameters used for optimization are crossover fraction 0.6, elite count 2, mutation function adaptive feasible and intermediate crossover. Two different population sizes $2\times n_{DV}$ and $4\times n_{DV}$ are explored, and the best result is retained. n_{DV} denotes the number of the decision variables. All the simulations are performed using Matlab 2012b on a desktop PC with Intel Core 2 Duo processor (2.83 GHz, 4GB RAM).

Optimum profile without dissolution

In order to present the motivation for the dissolution steps, first we find the optimal temperature profile without dissolution and compare the final CSD with the target. The optimization problem has been formulated as described in the previous section. As dissolution step is not included, the constraint for decision variables is taken as

$$0\,^{\circ}\mathrm{C} \le T_j - T_{j+1} \le 5\,^{\circ}\mathrm{C}. \tag{33}$$

The number of segments used in the study is $M = 25$. The results obtained after solving the optimization problem are shown in Figure 3. From Figure 3a, it can be seen that the CSD obtained from the final segment has a reasonably good match with the target, considering only the crystals grown from seeds. However, the amount of fines due to secondary nucleation (denoted by the peak in small size range) is significant. The fines mostly appear at the second half of the PFC as can be seen in Figure 3b where the evolution of the CSD along the PFC segments is presented. This is because of the fact that the optimal temperature profile increases supersaturation slowly at the initial segments and rapidly at the final segments (Figure 3c). From the operating curve in Figure 3d, it is further confirmed that the process never operates at the undersaturated region, and therefore, no dissolution takes place. Thus, for the system considered, optimal temperature profile without dissolution is unable to reduce

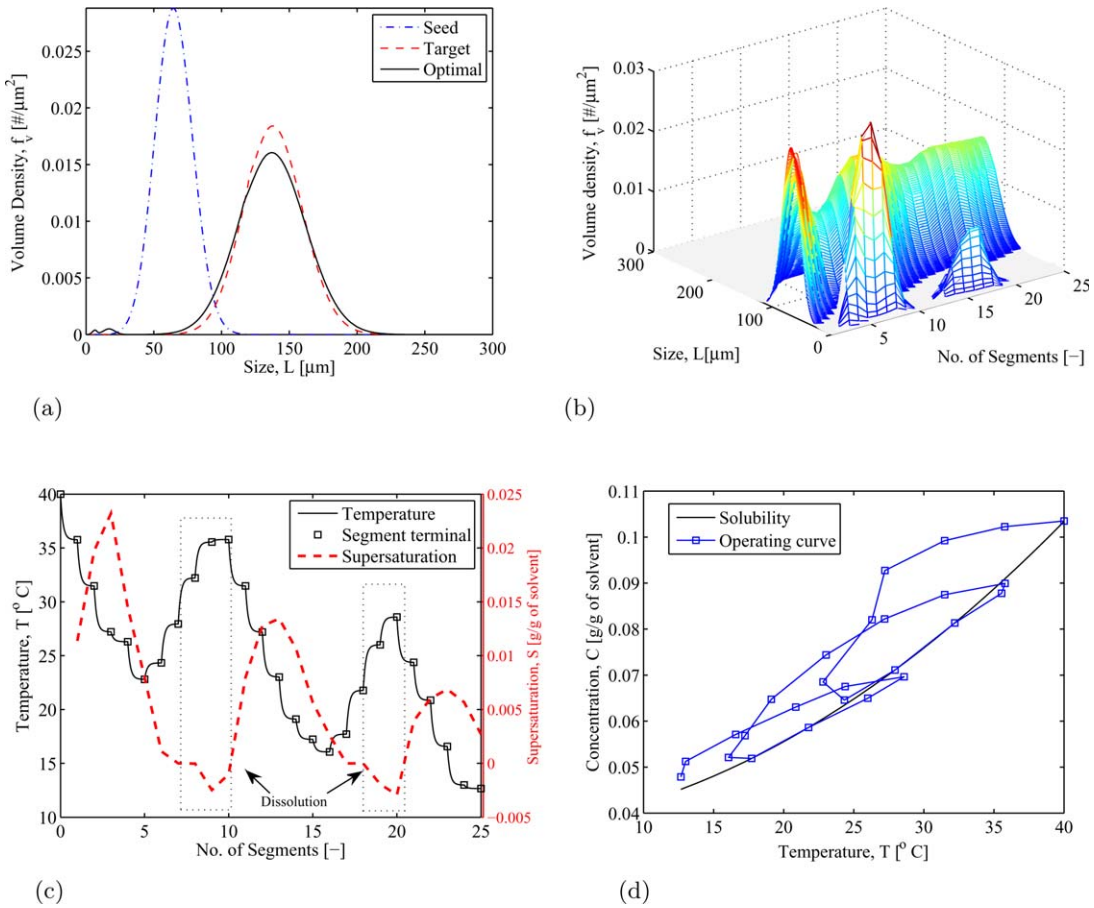

Figure 4. Optimization results when both growth and dissolution kinetics are size dependent.

The optimal profile includes both growth and dissolution steps to reduce the fines. (a) Final distribution. (b) Evolution of the CSD along the crystallizer segments. (c) Temperature and supersaturation profile. (d) Operating curve in the phase diagram. [Color figure can be viewed in the online issue, which is available at wileyonlinelibrary.com.]

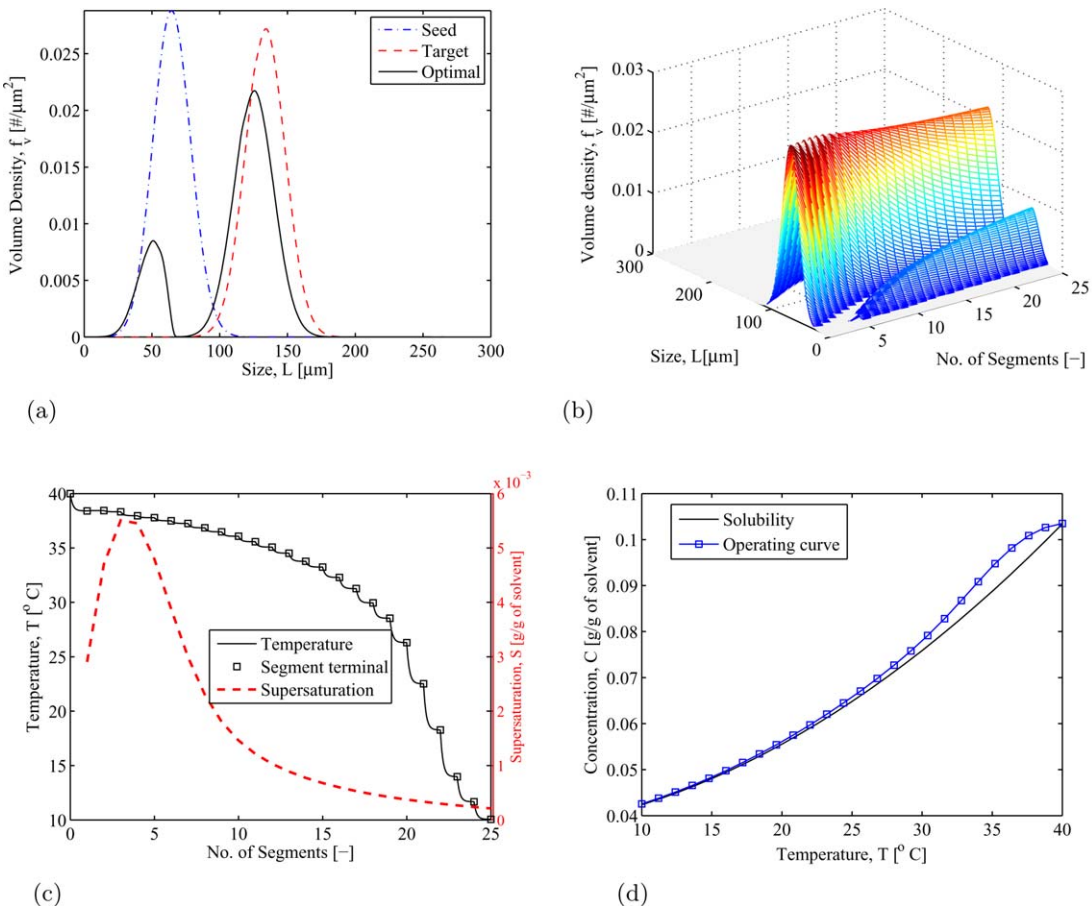

Figure 5. Optimization results when both the growth and dissolution kinetics are size independent.

The optimal profile does not include dissolution steps as it cannot provide a better match with the target CSD. (a) Final distribution. (b) Evolution of the CSD along the crystallizer segments. (c) Temperature and supersaturation profile. (d) Operating curve in the phase diagram. [Color figure can be viewed in the online issue, which is available at wileyonlinelibrary.com.]

fines to a desired level. The population size, number of generation required for convergence in GA, corresponding computation time, and objective functions are summarized in Table 2. In the next section, we present how the introduction of dissolution steps can bring significant improvement in achieving the target CSD.

Optimum profile with dissolution

Here, the dissolution steps are also introduced to obtain the optimal temperature profile. In order to perform a systematic study considering the effect of growth and dissolution kinetics, we consider the following three classes of crystallization systems:

1. Both the growth and dissolution kinetics are size dependent, that is, the larger crystals grow faster than the smaller ones and the smaller crystals dissolve faster than the larger ones.
2. Both the growth and dissolution kinetics are independent of crystal size.
3. Either growth or dissolution kinetics is size dependent.

Case 1: Both the Growth and Dissolution Kinetics are Size Dependent. When both the growth and dissolution kinetics are size dependent, the final CSD as shown in Figure 4a has a very good agreement with the target CSD. The amount of fines are reduced to a negligible quantity. In Figure 4b where the CSD along the PFC segments is shown, one can see that although significant amount of fines appear due to nucleation at the earlier segments, the fines are almost completely dissolved in the subsequent segments due to the dissolution steps. The temperature and supersaturation profiles are shown in Figure 4c where the dissolution regions are also marked. The dissolution steps can also be seen from Figure 4d where it is clearly shown that the operating curve indeed goes below the saturation curve by temperature cycling indicating that dissolution takes place. Note that similar temperature cycles have been shown to be beneficial for eliminating fines in batch crystallization,[8,13–15] where the cycles in the phase diagram are achieved by changing the temperature trajectory in time. In the case of PFCs, the similar dissolution cycles in the phase diagram are achieved by the spatial variation of temperature profile along the crystallizer. Summary of the optimization results are also shown in Table 2.

Case 2: Both the Growth and Dissolution Kinetics are Size Independent. Here, both the growth and the dissolution kinetics are taken to be independent of crystal size by setting $\gamma = 0$ and $q = 0$. The target CSD is obtained in a similar way as in the previous cases. However, the target CSD in Figure 5a is steeper than the previous cases, for example, in Figure 3a. This happens due the absence of size dependent growth, which has a dispersive effect on the CSD. Moreover, in order to make sure that the target CSD is located at similar size range as in Figure 3a, the growth rate parameter k_g in this study is taken to be two times larger as compared to

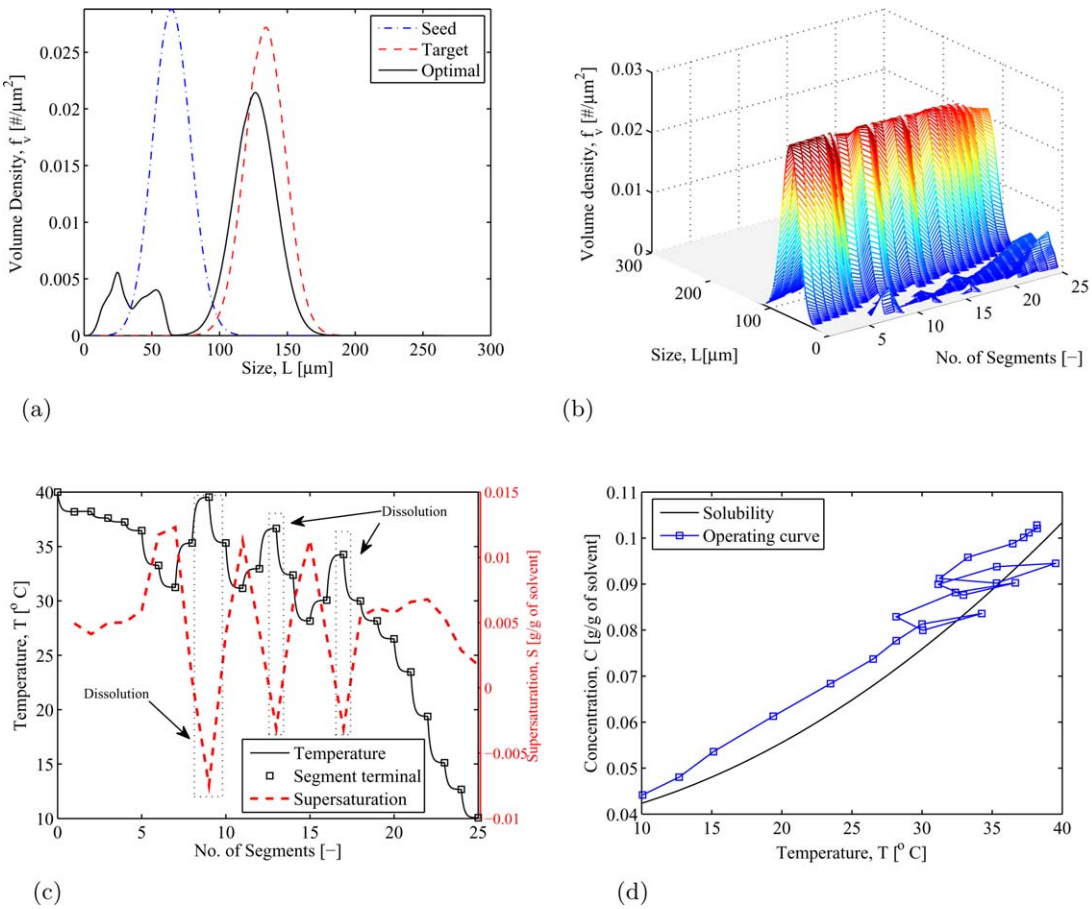

Figure 6. Optimization results when only dissolution kinetics is size dependent.

Better match with the target CSD is achieved than the case where both growth and dissolution kinetics are size independent. (a) Final distribution. (b) Evolution of the CSD along the crystallizer segments. (c) Temperature and supersaturation profile. (d) Operating curve in the phase diagram. [Color figure can be viewed in the online issue, which is available at wileyonlinelibrary.com.]

previous cases in order to compensate for the lack of size dependence. From Figures 5c,d, it can be seen that the optimal profile does not include dissolution steps even though the model includes the dissolution steps and the optimization allows increase in temperature. The optimal temperature profile in this case is very similar to the optimal profile without dissolution. This means that by considering dissolution steps, further improvement cannot be achieved for the size independent kinetics considered. The fines produced due to nucleation increases along the PFC segments which is indicated in Figure 5b. The CSD obtained from the final segment as seen in Figure 5a has a good agreement with the target CSD except for the fact that significant amount of fines are present due to the lack of the ability to remove fines via dissolution steps while achieving the target distribution. Thus, the fines cannot be reduced to the desired level with the current crystallization kinetics, that is, for the classes of crystallization systems for which both growth and dissolution kinetics are size independent.

Case 3: Only Dissolution Kinetics is Size Dependent. The kinetics considered in this section falls under the third class of crystallization systems. Only the dissolution kinetics is taken to be size dependent. The optimal temperature profile shown in Figure 6c is approximately a combination of the profiles for cases 1 and 2. A better match to the target CSD is achieved in Figure 6a in terms of fine dissolution than the size independent case. The phase diagram in Figure 6d points to the fact that the operating curve enters the undersaturated region in few instances at the middle segments where dissolution takes place. The effect of dissolution steps can be seen by looking at the evolution of the CSD along the segments in Figure 6b, which indicates disappearance of the three small peaks in the middle segments due to dissolution. However, the fines that appear at the final segments cannot be removed in this particular system. Similar conclusions are found when only growth kinetics is size dependent (results not shown here).

Effect of the number of segments

Here, we investigate the effect of number of modular segments on the target CSD. This is useful for process design where the optimum number of segments has to be found. We solve the optimization problem with size dependent growth and dissolution by varying the number of segments from 20 to 30. The results obtained are presented in Figure 7. From this plot, it can be seen that the value of the objective function is minimum when number of segments is 25 and 30. As, the results with 25 segments are found to be satisfactory, 25 segments are used in our studies.

Justification of using GA

In addition to the GA, a couple of other techniques, which use multiple starting points, are tested to solve the optimization problem for the case study with size dependent growth

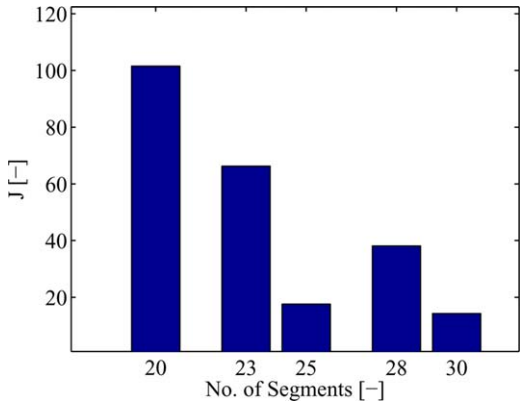

Figure 7. Plot showing objective function value as a function of number of segments.

[Color figure can be viewed in the online issue, which is available at wileyonlinelibrary.com.]

Table 3. Comparison of the Objective Function Values for Different Algorithms

Solver	J [-]
GA	17.57
GlobalSearch	34.59
MultiStart	19.42

and dissolution. The first one is the global search algorithm implemented in the "GlobalSearch" solver in Matlab.[26] This algorithm tries to combine the superior accuracy and feasibility-seeking behavior of gradient-based local NLP solvers with the scatter-search mechanism for global optimization. The other tested algorithm, implemented in the "MultiStart"' solver in Matlab, also uses multiple starting points with local NLP solver. The "active-set" algorithm is used as local solver in both techniques. However, the main difference between these two techniques is that "MultiStart" uses uniformly distributed start points within bounds, or user-supplied start points, whereas the "GlobalSearch" uses a scatter-search mechanism for generating starting points. The objective function values for these algorithm are summarized in Table 3.

It can be seen in Table 3 that the minimum value of the objective function is found with the GA solver. "MultiStart" solver also provides a solution which is close to GA. However, it is found to be computationally more expensive with n_{DV} starting points. Although global optimality is not guaranteed, GA is found to provide the best compromise between the computational efficiency and the chance to find the global optimum. Thus, we adopted GA as the approach used for solving the optimization problems.

Discussion on size dependent kinetics

Based on the findings in the simulation results, it can be concluded that the best results for fines removal is obtained for the class of the crystallization systems for which both the growth and dissolution kinetics are size dependent with the kinetic expressions of the form of Eqs. 7 and 8. The reason behind this observation can be explained with the help of Figure 8a, where the first peak of the CSD represents fine crystals due to nucleation and the second peak represents the large crystals grown from seeds.

The growth or dissolution process will shift the two peaks along the size axis in forward or backward directions, respectively. When the objective is to remove the fines without affecting the size of the larger crystals, then the distance η between the fines and the large crystals in the size space must be increased. In other words, there has to be a relative motion between the fines and large crystals. This is only possible for size dependent kinetics where large crystals have a higher growth rate than the smaller ones and smaller crystals have a higher dissolution rate than the larger ones as shown in Figure 8b. In this case, repeated dissolution and growth cycles will increase the distance η between the fine and coarse mode of the CSD. When dissolution is only size dependent in principle fine removal may be possible but the residence time may need to be adjusted by changing the flow rate of the PFC or by increasing the number of segments. For size independent kinetics, both the fines and seed will have a similar translational motion in the size space (i.e., no relative motion) and the distance η will not change. Thus, a fast or slow kinetics will only dictate how fast the translational motion would be without affecting the fines removal. In addition to the class of crystallization systems discussed, other classes can be analyzed similarly. For example, in the case of class of systems for which the empirical expressions for size dependent growth and dissolution kinetics are such that smaller crystals grow

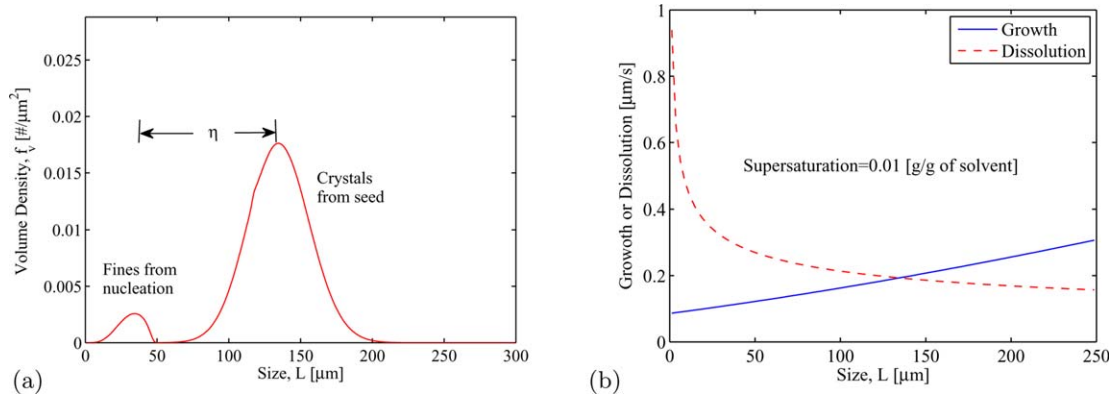

Figure 8. Schematic showing the condition required for fine dissolution.

(a) Size difference between fines and large crystals. (b) Growth and dissolution rates obtained with the parameters in Table 1 as a function of crystal size. [Color figure can be viewed in the online issue, which is available at wileyonlinelibrary.com.]

Table 4. Summary of the Optimization Results for Potash Alum-Water System

Case	Pop. Size [-]	No. of Gen. [-]	CPU Time [min]	J [-]
Without dissolution	80	170	54.43	329.40
With dissolution	80	200	379.21	38.32

faster than the larger ones[57] (e.g., diffusion-controlled growth) and the larger crystals dissolve faster than the smaller ones,[8] according to the discussion presented above, cycles of growth and dissolution will not increase the distance η and thus will be ineffective in removing fines. External fines removal unit may be required for such cases.

Proof of Concept for Potash Alum-Water System Using Experimentally Determined Kinetic Parameters

In this section, we consider the cooling crystallization of potash alum-water system in a PFC with 20 segments. The dimension of the PFC is the same as considered in the previous case studies. The dominant mechanisms present are growth, nucleation, and dissolution. Agglomeration and breakage are ignored. Size dependent growth and dissolution kinetics are observed in the experiment.[51] The expressions for these kinetics and experimentally determined parameters can be found in Shoji et al.,[51] and are not reproduced here for brevity. Based on the kinetics, this system belongs to the first class discussed in the previous section. The CSD for seeds are taken as

$$f_{\mathrm{n,seed}}\left[\#/\mathrm{m}^2\right]=\frac{0.266\times10^{10}}{15\times10^{-6}\sqrt{2\pi}}\exp\left(-\frac{\left(L-54\times10^{-6}\right)^2}{\left(15\times10^{-6}\right)^2}\right). \quad (34)$$

The target CSD considered here is again a unimodal distribution, which is obtained by following a linear cooling profile from $T_{\max}=40^{\circ}\mathrm{C}$ to $T_{\min}=20^{\circ}\mathrm{C}$ and arbitrarily setting nucleation to zero. However, here we compare the number-based CSD, as the nucleation kinetics for this system is not as dominant as the previous case studies. The solubility of potash alum in water is given by Eq. 32. Two scenarios for optimal temperature profile are investigated: first, only growth steps are considered and second, both the growth and dissolution steps are considered. The optimization problem is formulated in the same way as done in previous studies. The scaling factor is taken as $\lambda_i=10^{-25}$ m^2. The results obtained using GA with the parameters summarized in Table 4 are shown in Figures 9 and 10.

It can be seen that the objective function J is minimum when both the growth and dissolution steps are used. This is more evident from the plots of the final CSDs in Figures 9a

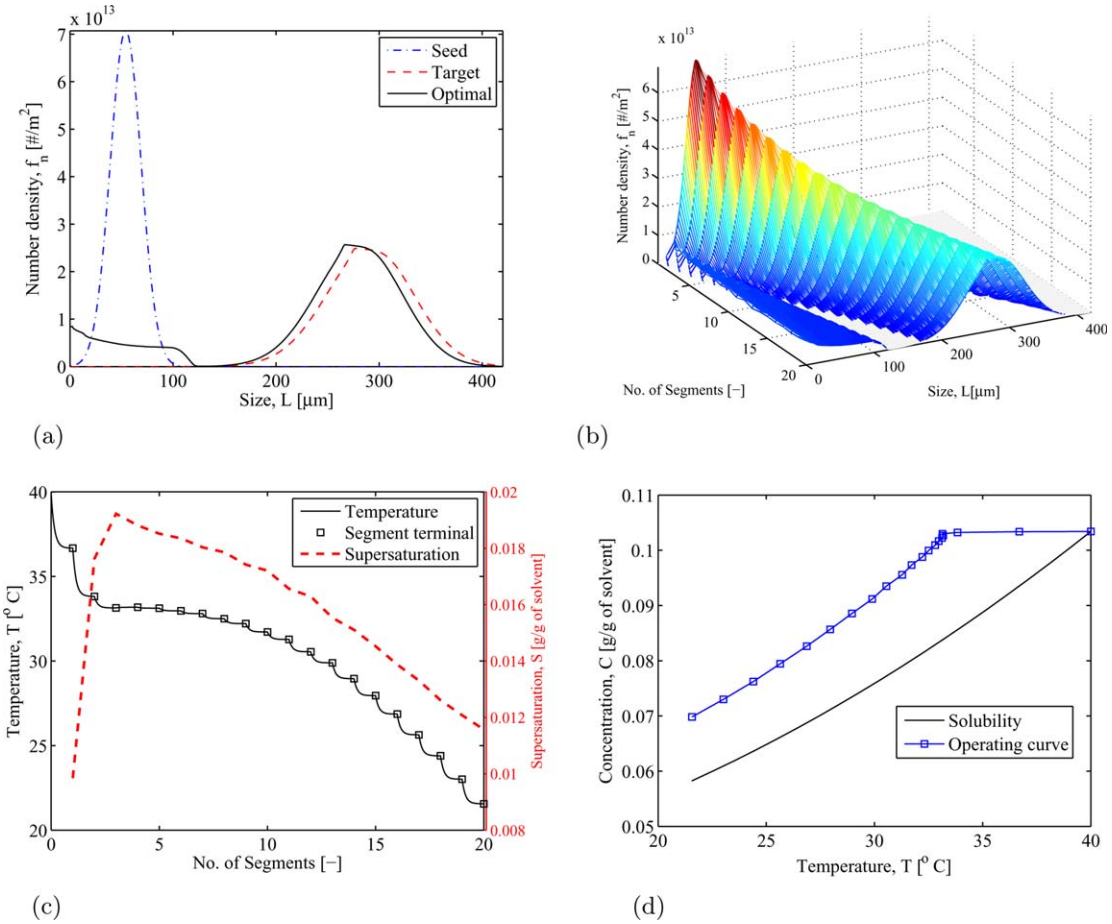

Figure 9. Optimization results for potash alum-water system when no dissolution steps are present.

Fines due to nucleation cannot be reduced significantly. (a) Final distribution. (b) Evolution of the CSD along the crystallizer segments. (c) Temperature and supersaturation profile. (d) Operating curve in the phase diagram. [Color figure can be viewed in the online issue, which is available at wileyonlinelibrary.com.]

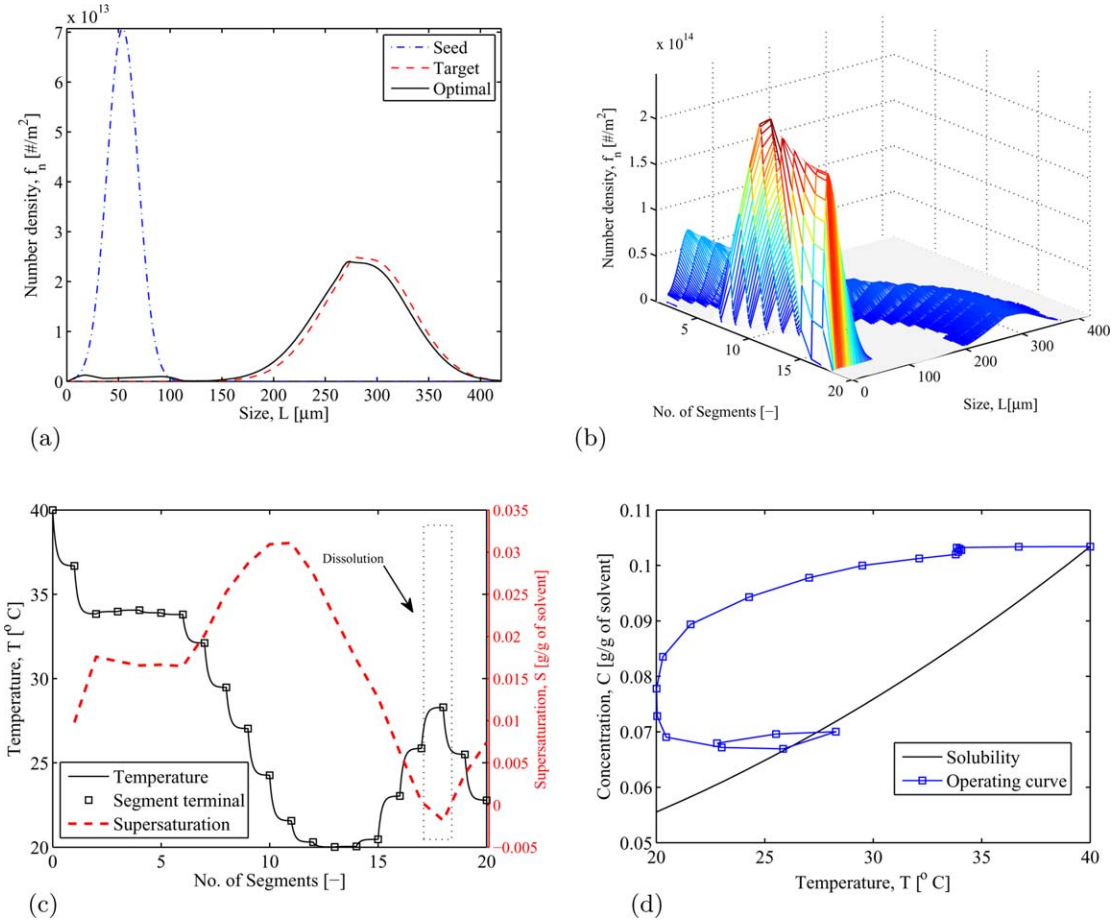

Figure 10. Optimization results for potash alum-water system when both growth and dissolution kinetics are size dependent.

The optimal profile includes both growth and dissolution steps to reduce the fines to a negligible quantity. (a) Final distribution. (b) Evolution of the CSD along the crystallizer segments. (c) Temperature and supersaturation profile. (d) Operating curve in the phase diagram. [Color figure can be viewed in the online issue, which is available at wileyonlinelibrary.com.]

and 10a. A much better match to the target CSD is obtained with the temperature profiles that includes dissolution steps, and the fines are also reduced to a negligible quantity. The dissolution steps can be clearly seen by looking at the temperature and supersaturation profiles in Figure 10c and the phase diagram in Figure 10d. The disappearance of the fines at the small size regions at the later segments, shown in Figure 10b, is due to the temperature cycling. Conversely, when dissolution steps are not present, the temperature profile (Figure 9c) is such that a relatively low supersaturation is maintained and the operating curve is close to the saturation curve in Figure 9d. These simulation results obtained with the experimentally determined parameters support our proposed hypothesis that dissolution steps are sometimes necessary for significant reduction of the fines due to nucleation. Satisfactory results in terms of fines reduction are obtained for the crystallization of potash alum-water system where both the growth and dissolution kinetics are size dependent.

Conclusions

Spatially distributed optimal temperature profile is proposed for the removal of fines in a continuous PFC. For the kinetic parameters considered, it is found that the optimal profile without dissolution is not able to reduce fines significantly. However, almost complete removal of the fines is achieved for the optimal profile with controlled dissolution steps and with size dependent kinetics. It is concluded that size dependent kinetics plays a key role in determining whether the dissolution steps would be useful in removing fines. Best result in terms of fines removal is obtained when both the growth and dissolution kinetics are size dependent.

Acknowledgments

Funding is acknowledged from the European Research Council under the European Union's Seventh Framework Programme (FP7/2007-2013)/ERC grant agreement No. [280106-CrySys].

Notation

A = cross sectional area of the PFC, μm^2
b = nucleation exponent, dimensionless
B_0 = nucleation rate, #/(m.s)
C = solute concentration, g/g of solvent
C_{sat} = saturation concentration, g/g of solvent
D = dissolution rate, μm/s
d = dissolution exponent, dimensionless

f_n = number-based distribution, #/μm^2
f_v = volume-based distribution, #/μm^2
g = growth exponent, dimensionless
G = growth rate, μm/s
k_b = nucleation parameter, #/(μm/s)
k_d = dissolution parameter, #/s
k_g = growth parameter, μm/s
k_v = volumetric shape factor, dimensionless
L = size of the crystal, μm
M = number of segments, μm/s
n_{DV} = number of decision variables, dimensionless
N = number of grid points, μm/s
p = exponent of crystal size for growth, dimensionless
q = number of segments, μm/s
Q = volumetric flow rate, μm^3/s
r = ratio of the slopes, dimensionless
S = absolute supersaturation, g/g of solvent
t = time, s
T = temperature, °C
x = axial distance along the crystallizer, μm
x_s = length of the PFC segment, μm

Greek letters

ϵ = small number, dimensionless
η = size difference between fine and large crystals, μm
γ = growth parameter, /μm
λ_i = scaling factor, μm^2
μ_3 = third moment of distribution, μm^3
ρ_c = density of the crystal, g/μm^3

Literature Cited

1. Alvarez AJ, Myerson AS. Continuous plug flow crystallization of pharmaceutical compounds. *Cryst Growth Des*. 2010;10(5):2219–2228.
2. Chen J, Sarma B, Evans JMB, Myerson AS. Pharmaceutical crystallization. *Cryst Growth Des*. 2011;11(4):887–895.
3. Lawton S, Steele G, Shering P, Zhao L, Laird I, Ni XW. Continuous crystallization of pharmaceuticals using a continuous oscillatory baffled crystallizer. *Org Process Res Dev*. 2009;13(6):1357–1363.
4. Gros H, Kilpiö T, Nurmi J. Continuous cooling crystallization from solution. *Powder Technol*. 2001;121(1):106–115.
5. Woo XY, Tan RBH, Braatz RD. Precise tailoring of the crystal size distribution by controlled growth and continuous seeding from impinging jet crystallizers. *CrystEngComm*. 2011;13(6):2006–2014.
6. Mullin JW, Nývlt J. Programmed cooling of batch crystallizers. *Chem Eng Sci*. 1971;26(3):369–377.
7. Aamir E, Nagy ZK, Rielly CD, Kleinert T, Judat B. Combined quadrature method of moments and method of characteristics approach for efficient solution of population balance models for dynamic modeling and crystal size distribution control of crystallization processes. *Ind Eng Chem Res*. 2009;48(18):8575–8584.
8. Nagy ZK, Aamir E, Rielly CD. Internal fines removal using population balance model based control of crystal size distribution under dissolution, growth and nucleation mechanisms. *Cryst Growth Des*. 2011;11(6):2205–2219.
9. Jones A. *Crystallization Process Systems*. Butterworth-Heinemann. Oxford, U.K.: Butterworth-Heinemann, 2002.
10. Jones AG, Chianese A. Fines destruction during batch crystallization. *Chem Eng Commun*. 1987;62(1–6):5–16.
11. Qamar S, Peter Elsner M, Hussain I, Seidel-Morgenstern A. Seeding strategies and residence time characteristics of continuous preferential crystallization. *Chem Eng Sci*. 2012;71:5–17.
12. Woo XY, Nagy ZK, Tan RBH, Braatz RD. Adaptive concentration control of cooling and antisolvent crystallization with laser backscattering measurement. *Cryst Growth Des*. 2008;9(1):182–191.
13. Abu Bakar MR, Nagy ZK, Saleemi AN, Rielly CD. The impact of direct nucleation control on crystal size distribution in pharmaceutical crystallization processes. *Cryst Growth Des*. 2009;9(3):1378–1384.
14. Saleemi A, Rielly C, Nagy ZK. Automated direct nucleation control for in situ dynamic fines removal in batch cooling crystallization. *CrystEngComm*. 2012;14(6):2196–2203.
15. Saleemi AN, Rielly CD, Nagy ZK. Comparative investigation of supersaturation and automated direct nucleation control of crystal size distributions using ATR-UV/vis spectroscopy and FBRM. *Cryst Growth Des*. 2012;12(4):1792–1807.
16. Fujiwara M, Nagy ZK, Chew JW, Braatz RD. First-principles and direct design approaches for the control of pharmaceutical crystallization. *J Process Control*. 2005;15(5):493–504.
17. Nagy ZK. Model based robust control approach for batch crystallization product design. *Comput Chem Eng*. 2009;33(10):1685–1691.
18. Nagy ZK, Aamir E. Systematic design of supersaturation controlled crystallization processes for shaping the crystal size distribution using an analytical estimator. *Chem Eng Sci*. 2012;84:656–670.
19. Worlitschek J, Mazzotti M. Model-based optimization of particle size distribution in batch-cooling crystallization of paracetamol. *Cryst Growth Des*. 2004;4(5):891–903.
20. Hu Q, Rohani S, Jutan A. Modelling and optimization of seeded batch crystallizers. *Comput Chem Eng*. 2005;29(4):911–918.
21. Sarkar D, Rohani S, Jutan A. Multi-objective optimization of seeded batch crystallization processes. *Chem Eng Sci*. 2006;61(16):5282–5295.
22. Ward JD, Mellichamp DA, Doherty MF. Choosing an operating policy for seeded batch crystallization. *AIChE J*. 2006;52(6):2046–2054.
23. Mesbah A, Landlust J, Huesman AEM, Kramer HJM, Jansens PJ, Van den Hof PMJ. A model-based control framework for industrial batch crystallization processes. *Chem Eng Res Des*. 2010;88(9):1223–1233.
24. Mesbah A, Huesman AEM, Kramer HJM, Nagy ZK, Van den Hof PMJ. Real-time control of a semi-industrial fed-batch evaporative crystallizer using different direct optimization strategies. *AIChE J*. 2011;57(6):1557–1569.
25. Ramkrishna D. Population Balances: Theory and Applications to Particulate Systems in Engineering. San Diego, CA: Academic Press, 2000.
26. Ugray Z, Lasdon L, Plummer J, Glover F, Kelly J, Mart R. Scatter search and local NLP solvers: a multistart framework for global optimization. *INFORMS J Comput*. 2007;19(3):328–340.
27. Hulburt HM, Katz S. Some problems in particle technology: a statistical mechanical formulation. *Chem Eng Sci*. 1964;19(8):555–574.
28. McGraw R. Description of aerosol dynamics by the quadrature method of moments. *Aerosol Sci Technol*. 1997;27(2):255–265.
29. Marchisio DL, Pikturna JT, Fox RO, Vigil RD, Barresi AA. Quadrature method of moments for population-balance equations. *AIChE J*. 2003;49(5):1266–1276.
30. Kariwala V, Cao Y, Nagy ZK. Automatic differentiation-based quadrature method of moments for solving population balance equations. *AIChE J*. 2012;58(3):842–854.
31. Gunawan R, Fusman I, Braatz RD. High resolution algorithms for multidimensional population balance equations. *AIChE J*. 2004;50(11):2738–2749.
32. Qamar S, Elsner MP, Angelov IA, Warnecke G, Seidel-Morgenstern A. A comparative study of high resolution schemes for solving population balances in crystallization. *Comput Chem Eng*. 2006;30(6–7):1119–1131.
33. Majumder A, Kariwala V, Ansumali S, Rajendran A. Fast high-resolution method for solving multidimensional population balances in crystallization. *Ind Eng Chem Res*. 2010;49(8):3862–3872.
34. Hermanto MW, Braatz RD, Chiu MS. High-order simulation of polymorphic crystallization using weighted essentially nonoscillatory methods. *AIChE J*. 2009;55(1):122–131.
35. Bouaswaig AE, Engell S. WENO scheme with static grid adaptation for tracking steep moving fronts. *Chem Eng Sci*. 2009;64(14):3214–3226.
36. Mahoney AW, Ramkrishna D. Efficient solution of population balance equations with discontinuities by finite elements. *Chem Eng Sci*. 2002;57(7):1107–1119.
37. Ganesan S, Tobiska L. An operator-splitting finite element method for the efficient parallel solution of multidimensional population balance systems. *Chem Eng Sci*. 2012;69(1):59–68.
38. Kumar S, Ramkrishna D. On the solution of population balance equations by discretization–III. Nucleation, growth and aggregation of particles. *Chem Eng Sci*. 1997;52(24):4659–4679.
39. Févotte F, Févotte G. A method of characteristics for solving population balance equations (PBE) describing the adsorption of impurities during crystallization processes. *Chem Eng Sci*. 2010;65(10):3191–3198.
40. Majumder A, Kariwala V, Ansumali S, Rajendran A. Entropic lattice Boltzmann method for crystallization processes. *Chem Eng Sci*. 2010;65(13):3928–3936.
41. Majumder A, Kariwala V, Ansumali S, Rajendran A. Lattice Boltzmann method for multi-dimensional population balance models in crystallization. *Chem Eng Sci*. 2012;70:121–134.

42. Majumder A, Kariwala V, Ansumali S, Rajendran A. Lattice Boltzmann method for population balance equations with simultaneous growth, nucleation, aggregation and breakage. *Chem Eng Sci*. 2012; 69(1):316–328.
43. Abegg CF, Stevens JD, Larson MA. Crystal size distributions in continuous crystallizers when growth rate is size dependent. *AIChE J*. 1968;14(1):118–122.
44. Kile D, Eberl D. On the origin of size-dependent and size-independent crystal growth: influence of advection and diffusion. *Am Mineral*. 2003;88(10):1514–1521.
45. McCabe WL, Stevens RP. Rate of growth of crystals in aqueous solutions. *Chem Eng Prog*. 1951;47(4):168–174.
46. Girolami MW, Rousseau RW. Size-dependent crystal growth-A manifestation of growth rate dispersion in the potassium alum-water system. *AIChE J*. 1985;31(11):1821–1828.
47. Lie-Ding S, Kris AB. Growth rate dispersion in batch crystallization. *AIChE J*. 1990;36(11):1669–1679.
48. Enüstün BV, Turkevich J. Solubility of fine particles of strontium sulfate. *J Am Chem Soc*. 1960;82(17):4502–4509.
49. Ståhl M, Åslund B, Rasmuson AC. Aging of reaction-crystallized benzoic acid. *Ind Eng Chem Res*. 2004;43(21):6694–6702.
50. Heffels SK, de Jong EJ. Improved operation and control of batch crystallizers. *AIChE Symp Ser*. 1991;87:170–181.
51. Shoji M, Eto T, Takiyama H. A kinetic study of the influence of modulated undersaturation operation on crystal size distribution in cooling-type batch crystallization. *J Chem Eng Jpn*. 2011;44(3):191–196.
52. van Leer B. Towards the ultimate conservative difference scheme. II. Monotonicity and conservation combined in a second-order scheme. *J Comput Phys*. 1974;14(4):361–370.
53. LeVeque RJ. Finite-Volume Methods for Hyperbolic Problems. Cambridge, UK: Cambridge university press, 2002.
54. Koren B. A robust upwind discretization method for advection, diffusion and source terms. *Notes Numer Fluid Mech*. 1993;45:117–138.
55. Roe PL. Characteristic-based schemes for the Euler equations. *Annu Rev Fluid Mech*. 1986;18(1):337–365.
56. Sbalzarini I, Müller S, Koumoutsakos P. Multiobjective optimization using evolutionary algorithms. *Proceedings of the Summer Program*. Stanford, CA: Center for Turbulence Research, Stanford University, 2000:63–74.
57. Gimbun J, Nagy ZK, Rielly CD. Simultaneous quadrature method of moments for the solution of population balance equations, using a differential algebraic equation framework. *Ind Eng Chem Res*. 2009; 48(16):7798–7812.

Manuscript received Mar. 25, 2013, and revision received Jun. 27, 2013.